THE ASTROPHYSICAL JOURNAL, 580:L161–L165, 2002 December 1

DISCOVERY OF NONTHERMAL X-RAY EMISSION FROM THE EMBEDDED MASSIVE STAR-FORMING REGION RCW 38

SCOTT J. WOLK,[1] TYLER L. BOURKE,[1] RANDALL K. SMITH,[1] BRADLEY SPITZBART,[1] AND JOÃO ALVES[2]
Received 2002 August 6; accepted 2002 October 17; published 2002 November 5

ABSTRACT

We report on results of a 96.7 ks *Chandra* observation of one of the youngest, most embedded and massive young stellar clusters studied to date in X-rays—RCW 38. We find a region of extended emission about 1.25 × 1.75 pc. The emission is consistent with synchrotron emission. The power index of the emission steepens toward the cluster core, implying that the magnetic field originates there. This is the first evidence of synchrotron emission filling a region of active star formation. The source of the necessary magnetic field is unclear. We measure the hydrogen column to the emission and find that $N_{\rm H}$ increases from 7.6×10^{21} to 1.61×10^{22} cm^{-2}, increasing from the northwest to the southeast quadrants of the cluster, consistent with near-infrared extinction data.

Subject headings: H II regions — ISM: individual (RCW 38) — stars: formation — X-rays: diffuse background — X-rays: stars

On-line material: color figure

1. INTRODUCTION

The southern star-forming region RCW 38 (Rodgers, Campbell, & Whiteoak 1960) is one of the brightest H II regions at radio wavelengths (e.g., Wilson et al. 1970). However, it has received scant attention, probably because of its southern location. The exciting source of the region, the O5 star IRS 2 (Frogel & Persson 1974; Smith et al. 1999), is surrounded by a cluster of embedded lower mass stars seen in the near-infrared (NIR; Ligori et al. 1994; J. Alves et al. 2002, in preparation). At a distance of 1.7 kpc (Beck, Fischer, & Smith 1991), RCW 38 is one of the nearest star-forming regions containing an early O star.

Dense molecular gas, as traced in CS $J = 2 \rightarrow 1$ emission (Zinchenko, Mattila, & Toriseva 1995), surrounds a centimeter radio ring (T. L. Bourke et al. 2002, in preparation) and appears to be confining the H II region. The central region is essentially free of dust and molecular gas (Smith et al. 1999; T. L. Bourke et al. 2002, in preparation). NIR observations (Frogel & Persson 1974; J. Alves et al. 2002, in preparation) show that the star-forming region lies behind $A_V \sim 10$ mag, so RCW 38 appears to be a blister H II region lying just inside the edge of a giant molecular cloud. Spectacular NIR Very Large Telescope (VLT) observations of the central 2.′5 (0.6 pc) reveal an embedded cluster around IRS 2 with a central density of ~850 stars arcmin^{-2} and a cluster age of $\lesssim$1 Myr (J. Alves et al. 2002, in preparation). A large percentage of the NIR sources show an infrared excess, indicating a large disk fraction.

We recently observed RCW 38 using the *Chandra X-Ray Observatory*. In this Letter, we report on the discovery of extended emission in the core of the cluster in addition to numerous point sources. The extent of the diffuse X-ray emission appears coincident with emission at centimeter and infrared wavelengths.

2. OBSERVATIONS

Chandra observed RCW 38 on 2001 December 10–11 for 96.7 ks using the front-illuminated Advanced CCD Imaging Spectrometer (ACIS) in the very faint mode. The telemetry was processed by the *Chandra* X-ray Center using standard data processing under version 6.4.0. The observation had a very uniform background rate. There was a brief (750 s) background spike. Data from this time were removed from all analyses. The ACIS focal plane was cold (−119.7°C). The CLEAN55 algorithm[3] was applied to further reduce background.

We use PWDetect[4] to identify sources across the entire I array. To do this, we first applied an exposure map and then binned for 2″ pixels per PWDetect requirements. Threshold significance is set to detect sources between 4 and 5.31 equivalent Gaussian sigmas, and the data are searched on scales of 0.″5–16″. With these settings, less than 1% of false detection is expected. In the central 2.′5 × 2.′5, about 190 X-ray sources are detected. Also noticeable in the central region is a higher than expected background rate. The total number of X-ray counts in the central region (sources removed) is 15,267. The total number of counts in a similar area about 5′ off-axis is 6234. It is clear that extended emission is present near the aim point, which is not present on other regions of the detector.

3. DIFFUSE X-RAY EMISSION

We immediately suspected that the cause of the enhanced background near the cluster core was diffuse X-ray emission. However, there were other possibilities, chiefly scattered X-rays and the weak emission from unresolved stars. To evaluate the effect of scattering, we consulted the *Chandra* calibration Web site,[5] which contains extensive calibration of the wings of point sources. The most conservative interpretation of the data indicates that less than 10^{-4} counts per source count are scattered more than 10″ from the source. We expect that less than 1 count may lie more than 10″ away from IRS 2 because scattering. There will also be some scattering due to interstellar dust; as much as 30% of the direct X-rays from IRS 2 may be

[1] Harvard-Smithsonian Center for Astrophysics, 60 Garden Street, Cambridge, MA 02138; swolk@cfa.harvard.edu, tbourke@cfa.harvard.edu, rsmith@cfa.harvard.edu, bspitzbart@cfa.harvard.edu.

[2] European Southern Observatory, Karl-Schwarzschild-Strasse 2, D-85748 Garching bei München, Germany; jalves@eso.org.

[3] See http://cxc.harvard.edu/cont-soft/software/clean55.1.0.html.

[4] See http://cxc.harvard.edu/cont-soft/software/PWDetect.1.0.html.

[5] See http://cxc.harvard.edu/cal.

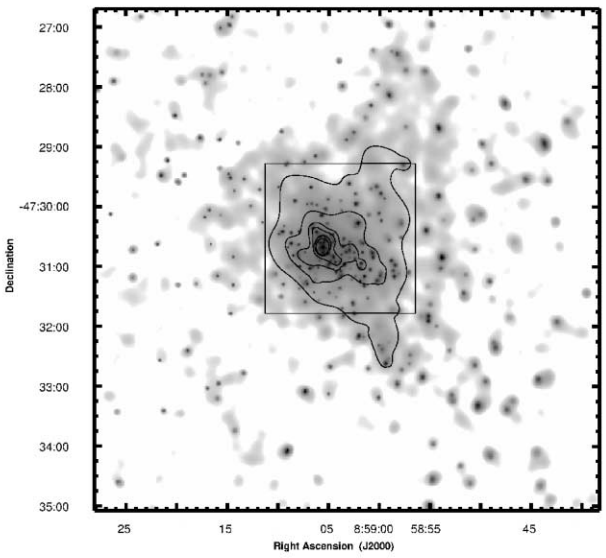

FIG. 1.—Smoothed image of the inner 9′ of the ACIS field. The data have been smoothed to about 1.′5 resolution, and the data are log-scaled. Contours represent 0.16, 0.4, 0.8, 1.6, 3, and 5 X-ray counts pixel^{-1}. Coordinates are J2000. The box is 2.′5 on a side and marks the region shown in Fig. 2. [*See the electronic edition of the Journal for a color version of this figure.*]

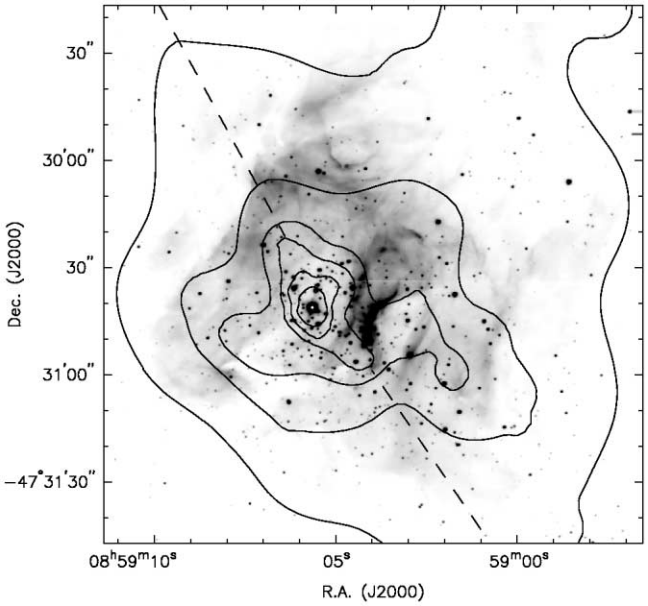

FIG. 2.—Diffuse X-ray contours overlaid on a K_s-band image taken with the VLT (J. Alves et al. 2002, in preparation). The image is about 2.′5 (1.25 pc) on a side. Contours represent 0.16, 0.4, 0.8, 1.6, 3, and 5 X-ray counts pixel^{-1} outer to inner and are well centered on IRS 2. The dashed line indicates the boundary between the northwest and southeast regions (see text).

scattered into a halo. This halo will be circularly symmetric and will be biased toward soft X-rays (Smith & Dwek 1998). We find hundreds of excess background photons more than 10″ away from IRS 2.

To investigate whether this excess could be caused by stellar X-rays from sources unresolved in this image, we used a deep NIR K_s-band image of the region taken with the VLT (J. Alves et al. 2002, in preparation). This image contains sources with K magnitudes as faint as 18.5 even in the most obscured regions (reaching the brown dwarf limit). We isolate starless regions in this image and compare the X-ray flux and spectrum in the starless regions with the rest of the enhanced background. There is no significant difference in the flux of the starless regions or in the flux of the general core of the cluster. We conclude that the heightened background is the result of faint diffuse X-ray emission.

To better visualize the extent and morphology of the emission, we created a smoothed rendering of the exposure-corrected image. This image was created from the event list described in § 2. The data in the event list were smoothed using the CIAO tool CSMOOTH. The smoothing kernel was allowed to range between 1″ and 7.′5. The result is shown in Figure 1. We repeat the exercise, removing sources detected with PWDetect so that we can better understand the morphology of the gas alone. The CIAO routine DMFILTH is used to extrapolate data into the holes left by the excised sources. While such extrapolated data are useful to guide examination regions, all analyses use the unadulterated event list.

3.1. *Morphology of the Extended Emission*

The region of emission extends about 2.′5 (1.25 pc) in the southeast-northwest direction and about 3.′5 (1.75 pc) in the northeast-southwest direction. Figure 2 shows a contour plot of the extended emission overlaid on the VLT K_s-band image. The falloff in count rate is roughly Gaussian, albeit with extended wings, from the center toward the northwest where strong differential absorption is not a factor. Although the emission is not circularly symmetric, we fitted the gas distribution with a Gaussian profile and find the FWHM $\sim 20''$.

Immediately striking is the coincidence of the peak of the diffuse X-ray emission with a hole in the extended K_s-band emission. Presumably, the K_s-band hole is formed by winds from IRS 2. The diffuse emission is filling the cavity traced by the K_s-band emission. There is a sharp cutoff of the extended emission to the southeast presumably caused by a large $N_{\rm H}$ column rendering the area opaque to X-rays. The events tend to be harder in the southeast than in the northwest (also an extinction effect). This mirrors a pattern seen in the NIR data in which the stars become redder toward the southeast, presumably because of dust extinction.

3.2. *Spectra of the Diffuse X-Ray Emission*

To characterize the background emission, we began by creating a contour map of a sourceless image. The typical background on the I array (away from the diffuse emission) was about 0.033 counts pixel^{-1} with a 1 σ variation of 0.001 counts pixel^{-1}. We define the emission region as the area on ACIS CCD-I3 with flux greater than this mean by 3 σ.

Source events from the emission region were filtered from the master event list. Energy data are extracted using CIAO binning on Pulse Invariant with a bin size of 5 (equivalent to about 75 eV). A weight map was then created by binning the events with a factor of 8. A weighted ancillary reference file (ARF) was made using the MKWARF tool, which selects appropriate FITS Embedded Function files for the chip location; this accounts for nominal charge transfer inefficiency and applies the weight map over the region of interest. Next, the tool MKRMF was run, again incorporating the weights file. A single, common background region consisting of the area on I3 that was at least 30″ away from the diffuse emission region was similarly extracted.

Spectral fitting allows us to check that the diffuse emis-

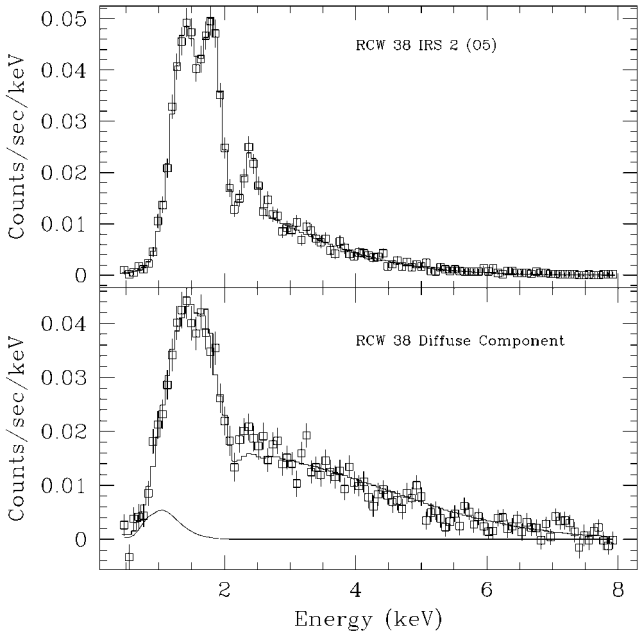

FIG. 3.—*Top*: Spectral fit to the central O star IRS 2. A thermal bremsstrahlung model with $kT = 1.65$ keV and $N_{\rm H} = 1.40 \times 10^{22}$ cm^{-2} is fitted to the data. Lines of Mg XI, Si XIII, and S XV are clearly seen. *Bottom*: Spectral fit of the entire diffuse emission. The data are fitted to a power law of index -1.59 with a small thermal component (*solid line*) and an absorption column of $N_{\rm H} = 9.5 \times 10^{21}$ cm^{-2}. No lines are prominent.

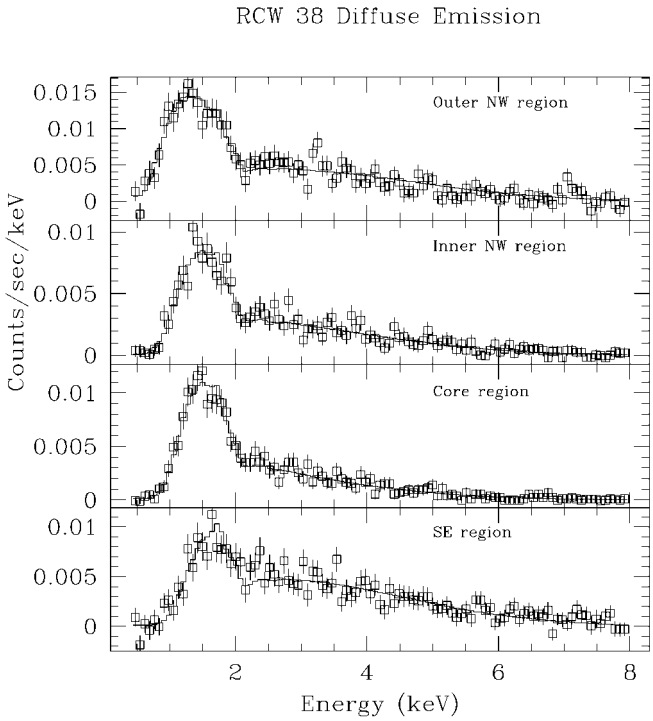

FIG. 4.—Spectra of the four subregions of the diffuse emission. The solid line is the fit of an absorbed power law with a thermal component (constrained to <1 keV). The $N_{\rm H}$ column increases by a factor of about 5, going from the northwest region at the top through the core to the southeast region at the bottom (see Table 1).

sion region is a unique source and not scattered light from the primary O star, IRS 2. We fitted events from IRS 2 using Sherpa, and the resulting spectrum is shown in Figure 3. The best fit to IRS 2 is a thermal bremsstrahlung model with $kT = 1.65$ keV and $N_{\rm H} = 1.40 \times 10^{22}$ cm^{-2}. More significantly, three lines are quite prominent here. The lines used in this fit, Mg XI at 1.36 keV, Si XIII at 1.86 keV, and S XV at 2.42 keV, tend to be the strongest lines in O stars (e.g., ζ Pup: Cassinelli et al. 2001; ζ Ori: Waldron & Cassinelli 2001; and Θ^1C Ori: Schulz et al. 2000). The reduced χ^2 statistic for this fit is 0.56. Error bars are 0.38 keV, and $N_{\rm H} = 2 \times 10^{21}$ cm^{-2}.

We fitted the spectrum of all of the events in the region of the diffuse emission region (point sources removed) after applying the weighted Redistribution Matrix Files and ARFs to a model fit. We could not find a stable fit to the data using a thermal bremsstrahlung model in Sherpa. We find that the thermal fits have a shallow minima with a temperature of about 2.0 keV and an absorption column of 7.0×10^{21} cm^{-2}. However, with a slight perturbation (<100 eV) in the initial temperature estimate, the temperature jumps to over 10 keV. The reason for this is clear from Figure 3. While the hard (>2.5 keV) emission from IRS 2 drops off very rapidly (exponentially), the hard extended emission falls off more slowly, almost linearly. The excess hard emission is evidence of a separate component rather than an X-ray halo. The X-ray halo would primarily be seen in soft (<2 keV) photons and should fall off as the inverse square of the energy.

If the hard spectrum seen in the diffuse emission is due to very hot ($T \gtrsim 10$ keV) electrons, the emission measure of this region, and thus the pressure, should be high. If the diffuse emission were under such a pressure, it should exhibit shocks, of which we see no evidence (such as line emission). To increase our sensitivity to lines, we reprocessed the event data using a charge transfer inefficiency correction algorithm (Townsley et al. 2000). Still, no lines were found. In addition, there is no sign of the cooler electrons toward the periphery that must exist if the electrons are accelerated in O star winds. Thus, we chose to fit the diffuse emission as the sum of a thermal bremsstrahlung plus a power law with extinction. For an initial guess, we fitted the data from 2 to 8 keV to a power law only since absorption beyond 2 keV should be nearly negligible. We then added the thermal and absorption components to the fit and simultaneously solved the three components. We find $N_{\rm H} = (9.5 \pm 1.8) \times 10^{21}$ cm^{-2} with a small thermal contribution with $kT = 0.195 \pm 0.035$ keV, which could be partially due to an X-ray halo from the point sources, but the flux is dominated by a power law with index $\Gamma = -1.59 \pm 0.12$ ($\chi^2_{\rm red} = 1.15$).

As shown in Figure 4, there is sufficient flux in the diffuse emission to subdivide it into four subregions defined by units of counts per pixel. Motivated by the NIR data and the color rendering of the X-ray data, both of which showed extinction tending to increase toward the southeast, we construct northwest, core, and southeast regions. There is sufficient flux to further divide the northwest into outer and inner regions. We defined the outer northwest contour to have between 0.16 and 0.8 counts pixel^{-1} and the inner northwest contour to have between 0.80 and 1.6 counts pixel^{-1}. The core region is defined as greater than 1.6 counts pixel^{-1}. Each of the four regions contains at least 1450 events due to diffuse emission.

Spectral fits to the four regions were made. We assumed that each region is dominated by power-law emission. As an initial guess, we used the parameters derived for the whole region, and holding the power-law index constant, a new column was derived. Then, using this set of new column densities, we re-derived all parameters. We set a maximum thermal component of 1 keV based on energy density considerations. The results are shown

TABLE 1
SPECTRAL FITS TO DIFFUSE X-RAY EMISSION

Region	Area (arcsec^2)	N_H ($\times 10^{22}$ cm^{-2})	Error	kT (keV)	Error	Norm.[a]	Γ	Error	Norm.[b]	χ^{2c}
Outer northwest	29,355	0.76	0.19	0.24	0.06	0.003	−1.32	0.19	6.58×10^{-5}	0.86
Inner northwest	2438	1.32	0.39	0.23	0.07	0.002	−2.08	0.20	9.25×10^{-5}	0.87
Core (power law)	453	1.48	0.13	1.00[d]	...	...	−2.77	0.19	2.02×10^{-4}	0.58
Core (APEC)	453	1.15	0.05	2.23	0.13	4.45×10^{-4}	...	...	...	0.59
Southeast	16,403	1.61	0.24	1.00[d]	...	...	−1.61	0.22	1.07×10^{-4}	1.00
Overall	48,649	0.95	0.18	0.19	0.04	0.010	−1.59	0.12	3.02×10^{-4}	1.15

[a] Normalized with units of $3.02 \times 10^{-15}/4\pi D^2 \int n_e n_I \, dV$.
[b] Normalized with units of photons keV^{-1} cm^{-2} s^{-1} at 1 keV.
[c] This is the reduced χ^2 Gehrels statistic. Each fit had 98 degrees of freedom.
[d] The maximum allowed thermal component was 1 keV.

in Table 1. The N_H increases from 7.6×10^{21} cm^{-2} in the outer northwest region to 1.48×10^{22} cm^{-2} in the core. The power-law index also steepens toward the core. The spectrum in the core region has a stable fit with a thermal plasma, albeit with low-metallicity abundances less than 0.04 solar. We fitted the core using the thermal plasma model APEC (Astrophysical Plasma Emission Code) and include the results in Table 1.

4. DISCUSSION

The diffuse emission in RCW 38 is dominated by a power-law spectrum, indicative of synchrotron emission. Synchrotron emission requires an electron population to be driven along a magnetic field. Astrophysically, this is most common along the expanding shock front of a supernova remnant or during violent accretion onto a compact object with a large magnetic field, neither of which is the obvious source in this case, although we note the existence of an anonymous barrel-type supernova remnant visible about 6′ north of the cluster center in the Two Micron All Sky Survey image of the region.[6] Furthermore, it is completely possible that there has previously been a supernova within this cloud; the 6 and 18 cm radio data show emission in the region (T. L. Bourke et al. 2002, in preparation), but the data are quite complex, and direct evidence of a supernova usually dissipates fairly rapidly (<10,000 yr).

In many ways, the emission here does resemble that of the shell supernova, such as SN 1006 (Dyer et al. 2001). This and several other shell supernovae are dominated by featureless, nonthermal emission, formed in a ring. SN 1006 has been well modeled using SRESC (Reynolds 1998), which also predicts the radio continuum. The SRESC fit to the subregions makes a prediction for a fairly flat radio spectrum, α between 0.12 and 0.37 ($S_\nu \propto \nu^{-\alpha}$). The SRESC models further predict that a radio flux due to synchrotron emission should peak near the core with a flux of 1.5 mJy at 1 GHz. At such low flux levels, the radio emission may be dominated by other flux sources, including the thermal radio continuum.

Diffuse emission has been seen in other star-forming regions including the Rosette Nebulae (Townsley et al. 2001), the Arches Cluster (Yusaf-Zadeh et al. 2002), and the NGC 3603 cluster (Moffat et al. 2002). The Orion Nebula cluster has about the same age and mass as RCW 38, but it has no evidence of extended emission and has a very low gas column, $N_H \sim 3 \times 10^{21}$ cm^{-2} (Feigelson et al. 2002; Flaccomio et al. 2003).

The emission from NGC 3603 has been characterized as thermal, $kT \sim 3.1$ keV, $N_H \sim 7.0 \times 10^{21}$ cm^{-2} (with a gradient of increasing column outward), and a total luminosity of 2×10^{34} ergs s^{-1} (Moffat et al. 2002). This group does find evidence of nonthermal radio emission from the proplyd-like objects within the cluster with radio spectral indices ranging from 0.1 to 0.5 (Mücke et al. 2002). For the Arches Cluster, Yusaf-Zadeh et al. fitted the diffuse emission to a two-temperature thermal model with temperatures of 800 eV and 6.4 keV. This second temperature can be interpreted as an iron line. Cantó, Raga, & Rodríguez (2000) and Raga et al. (2001) model the Arches Cluster by assuming a cluster of stars close enough that wind collisions in the dense stellar core would result in the production of strong X-rays. This model fits the Arches data quite well. A common theme among wind-driven models is that the emission should be primarily thermal bremsstrahlung. On this point, the RCW 38 data are in disagreement. At present, the cause of the synchrotron emission as the dominant diffuse X-ray emission within the RCW 38 H II region is unclear and poses a challenge to models of X-ray emission.

[6] See http://www.ipac.caltech.edu/2mass/gallery/rcw38atlas.jpg.

We are grateful to the anonymous referee for helpful comments and to Michael Corcoran for providing a working draft of Moffat et al. (2002). This project was funded by NASA grant G02-3015X and NASA contract NAS8-39073.

REFERENCES

Beck, S. C., Fischer, J., & Smith, H. A. 1991, ApJ, 383, 336
Cantó, J., Raga, A. C., & Rodríguez, L. F. 2000, ApJ, 536, 896
Cassinelli, J. P., Miller, N. A., Waldron, W. L., MacFarlane, J. J., & Cohen, D. H. 2001, ApJ, 554, L55
Dyer, K. K., Reynolds, S. P., Borkowski, K. J., Allen, G. E., & Petre, R. 2001, ApJ, 551, 439
Feigelson, E. D., Broos, P., Gaffney, J. A., III, Garmire, G., Hillenbrand, L. A., Pravdo, S. H., Townsley, L., & Tsuboi, Y. 2002, ApJ, 574, 258
Flaccomio, E., Damiani, F., Micela, G., Sciortino, S., Harnden, F. R., Jr., Murray, S. S., & Wolk, S. J. 2003, ApJ, in press
Frogel, J. A., & Persson, S. E. 1974, ApJ, 192, 351
Ligori, S., Moretti, A., Robberto, M., Guarnieri, M. D., & Zinnecker, H. 1994, Mem. Soc. Astron. Italiana, 65, 815
Moffat, A. F. J., et al. 2002, ApJ, 573, 191
Mücke, A., Koribalski, B. S., Moffat, A. F. J., Corcoran, M. F., & Stevens, I. R. 2002, ApJ, 571, 366
Raga, A. C., Velázquez, P. F., Cantó, J., Masciadri, E., & Rodríguez, L. F. 2001, ApJ, 559, L33
Reynolds, S. P. 1998, ApJ, 493, 375
Rodgers, A. W., Campbell, C. T., & Whiteoak, J. B. 1960, MNRAS, 121, 103
Schulz, N. S., Canizares, C. R., Huenemoerder, D., & Lee, J. C. 2000, ApJ, 545, L135

Smith, C. H., et al. 1999, MNRAS, 303, 367
Smith, R. K., & Dwek, E. 1998, ApJ, 503, 831
Townsley, L. K., Broos, P. S., Garmire, G. P., & Nousek, J. A. 2000, ApJ, 534, L139
Townsley, L. K., Feigelson, E. D., Broos, P. S., Chu, Y. H., & Montmerle, T. 2001, BAAS, 199, 124.04
Waldron, W. L., & Cassinelli, J. P. 2001, ApJ, 548, L45
Wilson, T. L., Mezger, P. G., Gardner, F. F., & Milne, D. K. 1970, A&A, 6, 364
Yusef-Zadeh, F., Law, C., Wardle, M., Wang, Q. D., Fruscione, A., Lang, C. C., & Cotera, A. 2002, ApJ, 570, 665
Zinchenko, I., Mattila, K., & Toriseva, M. 1995, A&AS, 111, 95